Final Draft
Manuscript available at: https://doi.org/10.1061/(ASCE)BE.1943-5592.0001954
Full citation: Wang, Y, Thrall, AP, Zoli, TP, Sun, S (2022) "Measuring Behavior of Long-span Bridges during Erection: Case Study of the Governor Mario M. Cuomo Bridge." Journal of Bridge Engineering, 27(12): 05022009

Measuring Behavior of Long-span Bridges during Erection: Case Study of the Governor Mario M. Cuomo Bridge

Yao Wang[a]; Ashley P. Thrall, Ph.D.[b]; Theodore P. Zoli, P.E.[c]; Shiyao Sun[d]

[a]PhD Candidate, Kinetic Structures Laboratory, Department of Civil & Environmental Engineering & Earth Sciences, University of Notre Dame, Notre Dame, IN 46556, USA. Email: ywang32@nd.edu

[b]Myron and Rosemary Noble Associate Professor, Kinetic Structures Laboratory, Department of Civil & Environmental Engineering & Earth Sciences, University of Notre Dame, Notre Dame, IN 46556, USA (corresponding author). Email: athrall@nd.edu

[c]National Bridge Chief Engineer, HNTB Corporation, 57th Floor, Empire State Building, 350 5th Ave, New York, NY 10118, USA. Email: tzoli@hntb.com

[d]Graduate Student, Kinetic Structures Laboratory, Department of Civil & Environmental Engineering & Earth Sciences, University of Notre Dame, Notre Dame, IN 46556, USA. Email: ssun4@nd.edu

Abstract

The design of long-span cable-stayed bridges is governed by dead and erection loads, as well as wind loading. Despite the importance of dead and erection loads, their impact on the behavior of built structures is unknown due to limitations in using conventional sensors (e.g., strain gauges) during construction. To address this knowledge gap, this paper introduces three-dimensional (3D) digital image correlation (DIC) as a method to measure the erection-induced and dead load behavior of bridges. DIC is a portable, non-contact photographic technique which relies on pattern recognition and photogrammetric triangulation principles to calculate strains. This paper demonstrates this method by measuring the behavior of the Governor Mario M. Cuomo Bridge – a twin-span, cable-stayed bridge – between two intermediate construction stages. The strains from the anchoring of six cables and the application of the tie down force were measured in the two edge girders, the end floor beam, and the supplemental longitudinal truss. Results indicate that the strains in the girders were similar in magnitude and approximately symmetrical in direction. Shear behavior was observed in the end floor beam between the north edge girder and the tie down. At the location of the shop weld of the end floor beam, an increase of strain was observed from the thicker side to the thinner side, with a change from flexure toward shear dominant behavior closer to the tie down. Measured results are compared with predictions from a 3D finite element model, further verifying this measurement technique. While this paper demonstrates this method for the Governor Mario M. Cuomo Bridge, DIC can be broadly used for the measurement of dead load and erection-induced strains, providing unprecedented information on behavior. Recommendations for implementing DIC for monitoring bridges during erection are provided.

Practical Applications

This paper introduces a method to measure the behavior of long-span bridges during erection. Specifically, a photographic measurement technique, known as digital image correlation, can track the strains induced between different stages of construction. Hardware includes two cameras that are mounted on a rigid bar, a sensor controller, and a data acquisition laptop as well as a power source (e.g., a portable generator). Photographs of bridge components, for which a pattern has been pre-applied, are taken at different stages. Then a software package calculates the strains based on pattern recognition. This technique overcomes the barriers of using conventional sensors (i.e., strain gauges) during erection, as the system does not need to remain on-site between erection stages and a constant power source is not required. This paper demonstrates this technique for the case study of the Governor Mario M. Cuomo Bridge, a twin-span cable-stayed bridge, but the technique could be used widely across the bridge industry.

Keywords: Erection-induced strain, long-span bridge, cable-stayed bridge, non-contact monitoring, digital image correlation, finite element modeling

Introduction

Dead and erection loading often govern the design of long-span cable-stayed bridges, as well as wind loading. Despite the relative importance of dead and erection loads to understanding behavior, structural health monitoring programs typically focus on live load behavior due to challenges in using conventional sensors during construction Conventional sensors, such as strain gauges, linear displacement transducers, and accelerometers, must take measurements continuously, require an on-site data acquisition system with continuous power, and can be fragile. All of these features makes these sensors challenging to use during heavy construction practices. In contrast, the non-contact, photographic measurement technique digital image correlation (DIC) is well-suited to measure the behavior of a bridge during erection. Specifically, the portable DIC system - comprised of cameras mounted on a rigid bar, a sensor controller, and a data acquisition laptop - can acquire photographs of members at different stages of construction. Based on pattern recognition and photogrammetric triangulation principles, the three-dimensional (3D) DIC algorithm can then calculate relative changes in strains in the photographed regions between the stages of construction. Thus, no equipment remains on-site and continuous measurements are not necessary. A major advantage is also that DIC measures strains over an entire field of view (FOV) and the direction of strain within this FOV can be determined in post-processing. Conventional sensors provide data at only discrete locations in a direction that is pre-determined. Thus, DIC is capable of capturing the complex strain fields and gradients that can occur from the erection of long-span bridges.

This paper demonstrates the capability and the value of using 3D DIC to measure the erection-induced strains in long-span bridges through monitoring the behavior of the Governor Mario M. Cuomo Bridge between two intermediate stages of construction (Figure 1). The Governor Mario M. Cuomo Bridge is a twin span, cable-stayed bridge over the Hudson River between Tarrytown, NY and Nyack, NY, located north of New York City, NY. It was built to replace the Tappan Zee Bridge, which carried more traffic than it was designed for, had higher rate of accident and congestion due to its narrow lanes and the absence of shoulders, and needed expensive maintenance (Han et al. 2019; Barbas and Paradis 2019). The bridge was designed to have a 100-year service life (Han et al. 2019; Barbas and Paradis 2019). A sophisticated monitoring system with more than 300 sensors has been installed to monitor the completed structure after erection [e.g., temperature change, displacement; see Han et al. (2019) for details]. As a transportation project, the bridge was among the largest single design-build contracts in the United States (The New NY Bridge, About the Project 2020). During the construction, engineers came up with innovative solutions for different challenges [e.g., complicated foundation construction, design of the prestressed deck panel for approach spans (Han et al. 2019; Barbas and Paradis 2019)]. The westbound lanes were opened to traffic in August, 2017, and the eastbound lanes were opened to traffic in September, 2018 (The New NY Bridge, Iconic opening 2018). The main span is 366 m (1,201 ft.) and the side span is 157 m (515 ft.) with a vertical clearance of 41.8 m (137 ft., [2]).

This paper presents the measured strains that were induced by cable anchoring forces applied on edge girders near the end floor beam from six cables (three on each plane) and the tie down forces applied on the end floor beam (Figure 2). Due to the asymmetry of the middle span and the side span, tie down forces were applied at the end floor beams of the side spans. This study focuses on understanding the behavior of the east end floor beam of the eastbound bridge and the adjacent members. The monitored members included (1) two edge girders, (2) the east end floor beam, and (3) a supplemental longitudinal truss. The monitored components were comprised of high-strength steel with 485 MPa (70 ksi), 517 MPa (75 ksi), and 485 MPa (70 ksi) yield strength for the edge girders, the end floor beam, and the supplemental longitudinal truss, respectively. This is the first time that DIC has been utilized to monitor the behavior of a long-span bridge during erection.

Objectives

The objective of this paper is to demonstrate the capability and the value of implementing 3D DIC to measure the erection-induced strains in long-span bridges. Specifically, this research measures the surface strains in the (1) two edge girders, (2) the end floor beam, and (3) a supplemental longitudinal truss of the Governor Mario M. Cuomo Bridge from cable anchoring forces and tie down forces (Figure 1 and Figure 2). Measured results of three locations of the end floor beam are compared with predictions from a 3D finite element (FE) numerical model, providing a means of verifying the measured results. Research results provide unprecedented data on the complicated behavior of the bridge during erection – a governing case for the design of many long-span bridges.

Background

Measured Behavior of Long-span Bridges during Erection

There are only a few examples in which the behavior of long-span bridges during erection have been monitored. Examples of monitoring the behavior of truss bridges during erection includes measuring the reaction forces using hydraulic jacks (Koller 1997), stress in members using Pfender equipment (Koller 1997), strain in members using gauges (Kleinhans 2010; Weinmann and Huey 2015; Malite et al. 2018), and distortion using tilt meters and laser distance sensors (Kleinhans 2010; Weinmann and Huey 2015). Dead load stresses of existing truss structures have also been measured using accelerometers that monitor the frequency of vibration of components under ambient conditions (Kleinhans 2010; Weinmann and Huey 2015). During the strengthening and widening of the Tamar suspension bridge, the deck vertical displacement was monitored through a hydraulic level sensing system, the displacement of the tower was monitored using an electronic distance measuring device, and the force in the new stay cables were monitored by strain gauges (Koo 2013). In arch construction, the strain in the arch and other structural components have been measured using strain gauges (Wu and Chen 2008; Zhou et al. 2017) and vibrating string extensometers (Hu et al. 2012), the force in tie bars has been measured using vibrating-wire force gauges (Wu and Chen 2008), the tensile forces in suspenders and prestressing cables have been measured using accelerometers and tension rings (Zhou et al. 2017), the deformations have been tracked (Wu and Chen 2008), the deck profile has been measured using pressure transducers (Zhou et al. 2017), and the dynamic behavior has been investigated through accelerometer measurements (Zhou et al. 2017).

As cable-stayed bridges are highly indeterminate, any type of construction and fabrication tolerance could lead to changes in the in-service behavior of the final system

(Yamamoto and Kitahara 1986; Casas and Aparicio 1998; Han and Sun 2003). Due to the relative higher tolerance in the construction and the unavoidability of construction errors, it is important to monitor the internal forces and geometry of the structure during the erection process. Therefore, numerical methods have been developed (Yamamoto and Kitahara 1986; Casas and Aparicio 1998; Han and Sun 2003; Shahawy and Arockiasamy 1996a; Schlaich 2001; Somja and de Ville de Goyet 2008; Oliveira Pedro and Reis 2010) and field monitoring systems (Casas and Aparicio 1998; Han and Sun 2003; Shahawy and Arockiasamy 1996b; Barton et al. 1990) have been implemented to monitor and understand the structural behavior during the erection process. Shahawy and Arockiasamy (1996a,b) monitored the behavior of the Sunshine Skyway Bridge during and after construction. Carlson strain meters were used to measure the concrete strains in selected pylon and pier sections, and bridge segments. Thermal couples were also used to measure the temperature of selected bridge segments and pylon sections. A method was developed, validated by the measured concrete strains in the pylons and bridge segments, to predict the behavior of the bridge during different stages of erection. Casas and Aparicio (Casas and Aparicio 1998) monitored the behavior of the Alamillo Bridge during erection and after completion. The bridge was instrumented by multiple types of sensors (e.g., strain gauges, extensometer, load cells, and pressure transducers) to understand the behavior of different members (e.g., both steel and concrete parts of the deck, reinforced concrete pylon, and forces in the cables). The field measurements not only provided the actual behavior of the bridge, but also helped update the model to achieve better agreement between measured data and predictions. Barton et al. (1990) used mechanical and electrical resistance gauges to monitor the strains induced by cable tensioning and post-tensioning in the deck segments of a segmentally-erected, post-tensioned box girder cable-stayed bridge. The main span and the two adjacent approach spans were instrumented. The measurements of the mechanical strain gauges in the deck indicated that cable tensioning had more effect on the behavior of the segment farther away from it and shear lag was also observed. Han and Sun (2003) used accelerometers to measure the cable forces, and strain gauges to measure the concrete stresses in the girder and pylons of the Yamen Bridge. The measured cable forces were compared to the predictions to perform parameter identification. The measured concrete stresses were used as an indicator of construction safety. Existing research shows the importance of understanding the behavior of cable-stayed bridges during erection. However, conventional instrumentation is commonly used, which is only capable of measuring strain at one point in one direction instead of giving a full-field strain map. Furthermore, the direction of the strain cannot be predicted easily, given the complicated force environment during the erection, which makes it harder to determine the behavior of the structure by using conventional instrumentation.

Monitoring Bridges using DIC

DIC has been widely implemented in different fields (Sutton et al. 2009, Pan et al. 2009). Although there are various applications of DIC in structural engineering (McCormick and Lord 2012; McGinnis et al. 2012; Sony et al. 2019; Mathew et al. 2018; Kim et al. 2020; and Molina-Viedma et al. 2020), its application in bridge engineering is limited. Wang et al. (2021) summarizes the different types of bridges (e.g., steel girder bridges, suspension bridges) that have been monitored by DIC, as well as the types of measurements (e.g., displacements, strains). To date, the application of DIC for monitoring cable-stayed bridges has been limited to monitoring the displacements of members. Gikas et al. (2014) and Piniotis et al. (2016) used two-dimensional (2D) DIC, among other types of sensors, to monitor the displacement of the deck, the cables, and the pylon of an existing single span cable-stayed bridge under static loads, dynamic loads, and ambient vibration. The goal was to verify the structural integrity of the tested bridge and to use the measured data sets as references for research related to bridge health monitoring. Only the deck displacement measured by DIC was presented, which was used to identify the modes of the deck. Kim et al. (2013) and Kim et al. (2017) used 2D DIC to measure the displacement of cables under traffic of an already built cable-stayed bridge. The measured data gave dynamic information on the cables which was used to estimate the forces in the cables. Ye et al. (2013) developed a 2D DIC system, which was used to monitor the displacement of a cable-stayed bridge under truck loading. This body of existing research was performed on already constructed cable-stayed bridges, as opposed to cable-stayed bridges during construction which is the focus of this research. The existing research used 2D DIC, which can capture in-plane displacements and strains. This is in contrast to 3D DIC, which can also capture out-of-plane displacements and strains.

There is no published research on the application of DIC to measure the behavior of long-span bridges during erection. This paper presents the first implementation of DIC in monitoring the erection-induced strain of a long-span bridge, with a focus on behavior between two intermediate stages of construction.

Monitoring Program

Monitoring Approach

The monitoring was performed in two separate trips to the bridge site. The purpose of the first trip was to use DIC to capture initial reference frames at an initial stage of construction. The purpose of the second trip was to measure the relative change in strain from the initial reference frames to a later stage of construction.

The first trip was from July 29, 2017 to August 12, 2017. During this time, the end floor beam was not tied down to the pier. Of the three pairs of cables studied, only one pair (the furthest of the three from the end floor beam) was installed to its initial stress. The other two pairs were not yet installed. DIC patterns (which will be discussed in Digital Image Correlation Section) were applied at each monitoring location, and DIC reference frames were taken.

The second trip was from October 14, 2017 to October 19, 2017. Between the two trips, all three pairs of cables were anchored, and the end floor beam was connected with the pier through the tie down. DIC photographs were taken again for each monitoring location. The strains induced by the cable anchoring forces and the tie down forces were calculated by comparing the DIC photographs taken during the second trip to the ones taken during the first trip.

Five locations of the eastbound bridge (all located near the east end floor beam) were monitored: (1) the south edge girder (Figure 2a and c, Figure 3), (2) the north edge girder (Figure 2a and c, Figure 3), (3) the east end floor beam between the north edge girder and the tie down (Figure 2a and b, Figure 4), (4) the shop weld at which the thickness of the web changes from 0.0381 m (1.5 in.) to 0.0222 m (0.875 in.) of the east end floor beam (Figure 2a and b, Figure 5), and (5) the supplemental longitudinal truss (Figure 2a and d, Figure 6).

Digital Image Correlation

DIC is a non-contact, non-destructive photographic measuring technique that calculates full-field displacements and strains via image correlation and photogrammetry (Schmidt et al.

2003a,b). A stochastic grayscale pattern is required to first be applied to monitored regions since DIC relies on pattern recognition. Photographs are taken at an initial strain state (the aforementioned reference frames) and after a load is applied. The captured photographs are divided into pixelated regions called facets and the center of each facet is a data point. The same facet is found in both cameras using pattern recognition and image correlation. Then photogrammetric triangulation principles are used to calculate the 3D coordinates of the center of each facet. All of the facets are tracked through a complete image series to yield full-filed 3D displacement and strains (Schmidt et al. 2003a). Before testing, the system needs to be calibrated so that the relative position of the two cameras and the distortion of the lenses can be determined.

Pressure-activated adhesive tape investigated by Wang et al. (2019) was used for the patterning strategy in this study due to its compatibility with painted steel, short application time, and long durability. That laboratory study performed by the authors compared DIC measurements using a pattern applied via pressure-activated adhesive tape with measurements taken by a strain gauge and an extensometer, as well as finite element (FE) numerical predictions. The results indicated strong agreement among the DIC data, measured data from conventional instrumentation, and FE predictions. Additionally, this prior research verified that the pressure-activated adhesive tape is compatible with the same protective multilayer paint coating used for the Governor Mario M. Cuomo Bridge. In Wang et al. (2022), the authors also demonstrated agreement between strain gauge measurements and measurements taken via DIC (using the same pressure-activated adhesive tape pattern strategy) for the field monitoring of a steel girder bridge, further validating this approach.

The 3D DIC system used in this study consists of two 2448 x 2050-pixel cameras with 12 mm (0.472 in.) lenses. Each camera is mounted securely on a rigid bar supported by a tripod to ensure that the relative position of the cameras remains fixed during calibration and measurement (Figure 7). The ARAMIS (ARAMIS User Manual 2017) software was used to control the system to acquire frames and to calculate strains after the frames were taken. This software package has a resolution of 100 microstrain (ARAMIS User Manual 2017). The FOV used for this research was about 2280 mm x 1990 mm (89.8 in. x 78.3 in.). The gauge length used was 0.0754 m (2.97 in.). Figure 7 shows the implementation of DIC in the field, monitoring the north edge girder.

This research used 3D DIC as opposed to 2D DIC. 2D DIC uses a single camera that is parallel to the measurement area to measure planar strains and displacements. In comparison, 3D DIC uses two cameras, and is thus able to determine depth and out-of-plane deformations through triangulation (Schmidt et al. 2003a,b, Schmidt and Tyson 2004, Trilion 2020). It is advantageous to use 3D DIC for bridge monitoring as it may be difficult to ensure that the DIC system is parallel to the measurement surface in the field, especially if measurements are taken at different times and the system is removed and returned to site.

While DIC can be used to measure both displacements and strains, this research focused only on measuring strains as the displacements of interest for the erection of a cable-stayed bridge (e.g., global deck displacements during cable tensioning) could not be captured from the available access areas.

Note also that the DIC cameras could not stay in their location during erection due to the construction activities on site. Thus, the cameras were removed from site between the two trips. Between the two trips, the camera mounts on the rigid bar were not changed to ensure that the relative camera position and angle was the same for both sets of measurements. Detailed field notes and measurements were taken during the first trip such that the setup location used for the reference frames could be replicated for the measurements taken in the second trip. Even with this great care, it would be impossible to exactly replicate the locations. Thus, the ARAMIS software package capability to remove rigid body motion was utilized to calculate the measured strains. This, however, would preclude the calculation of global displacements.

Data Processing

Noise exists in DIC measured strains and could result from (1) low quality of the acquired images (e.g., caused by irregular lighting environment and low quality patterns), and (2) inaccuracy of correlation process (related to calibration procedure and software) (Baldoni et al. 2016). Different approaches have been developed to minimize the noise (e.g., Wang et al. 2019 and Wang et al. 2021; Baldoni et al. 2016; Palanca et al. 2016; Gonzalez and Woods 2008). The approach developed in Wang et al. 2021 is used to reduce the noise in DIC measurement. Area averaging was valid in this study, as the height of the average area was less than 25% of the height of the member except for the supplemental longitudinal truss. Therefore, the strain within the average area had a relative uniform distribution.

The white boxes in each data figure indicate the area used for area averaging in each monitored location. Data near the edges was excluded due to high levels of noise in this region as well as the development length required by the pressure-activated adhesive tape to measure strains in steel (Wang et al. 2019). For edge girders (Figure 3) and the shop weld of the end floor beam (Figure 5), larger regions were excluded due to data loss. The triangular part of the pattern in between the north edge girder and the tie down (Figure 4), and the pattern on the supplemental longitudinal truss (Figure 6) was excluded for simplicity.

It should be noted that between the two trips, a portion of the pattern on the end floor beam between the north edge girder and the tie down was accidentally removed by a contractor who did not understand the technique being implemented (as shown in Figure 4). This unexpected accident demonstrates the importance of proper communication with contractors for implementation of DIC so that the pattern remains intact between different measuring dates. Fortunately, the strong bond between the pattern and the girder made it difficult to remove the entire pattern. Based on visual observation, no damage was found to the coating on the steel in the area where the pattern was removed, which demonstrates that applying or removing the pattern does not affect the coating. Although the whole pattern was not available, the rest of the pattern still provided adequate information on the behavior of this region. This demonstrates the high redundancy of DIC compared to conventional instrumentation (e.g., if a strain gauge is damaged, no data can be retrieved).

Reference frames taken during the first trip can be used to quantify the noise level. Two standard deviations of the reference frames are used as the noise level in this study. For all monitored locations, the noise level (taken as two standard deviations) is less than 123 microstrain, which is similar to the noise level of tests performed in a laboratory.

As erection causes complicated strain directions, a method to find the principal strains was needed. Unlike the fixed measured strain direction of conventional instrumentation, the strain direction in DIC can be changed after the photographs have been acquired. Therefore, a strain directionality analysis technique was developed. First, the strain in the longitudinal and vertical axes were calculated. Then the axes were rotated counterclockwise by 5°, and the strains in the new axes were calculated. This step was repeated until the original axes were rotated by

90°. Then the pair of the strains which gave the maximum and minimum strains was used to find the principal strain directions and magnitudes.

Finite Element Numerical Modeling

A local 3D FE numerical model of the end floor beam was built in ABAQUS/Standard (ABAQUS 2022) as a means of verifying the measured strains between two intermediate construction stages. This FE model will be used to validate DIC measurements and is not reflective of in-situ performance.

The FE model (Figure 8) is based on the free body diagram shown in Figure 9, which includes part of the north edge girder and half of the end floor beam. Boundary conditions include: (1) translation restrained in z-direction along web and flange of edge girder, (2) translation restrained in the x-direction along web and flange of end floor beam, and (3) translation restrained in the y-direction at the four locations where the tie down cables are attached to the end floor beam. To achieve a representative stress state, a design bearing reaction force, *B* of 13,400 kN (3,020 k) and a design shear force in the edge girder, *V* of 3,570 kN (780 k) are applied. All components are modeled using S45 or S3R (four- or three-node) shell elements. The steel is modeled as linear elastic with a Young's modulus of 200 GPa (29,000 ksi). Geometric linearity is assumed.

Comparisons between the measured principal stresses and the principal stresses from the FE model will be made. In the FE model, the principal stresses are found for the approximate region of which the DIC measurements were average. The angle of the principal stresses was then determined using Mohr's circle. Note, however, that the results are shown for the angle, Θ as defined in each of the data figures.

Results

Edge Girders

Stresses [converted from the measured strains by assuming a Young's modulus of 200 GPa (29,000 ksi)] in symmetrical locations (Figure 2a and c) on the south and north edge girders close to the end floor beam due to the anchoring of six cables (three on each plane) and the application of the tie down forces were measured. Figure 3 shows the principal stresses measured on the webs of the two edge girders. In this paper, negative indicates compression and positive indicates tension. Compressive stresses were measured in both girders, which was expected for the edge girders of a cable-stayed bridge. The direction of the principal stresses was also expected (65° for the south edge girder and 30° for the north edge girder), considering the direction of the resultant of the cable anchoring forces and the tie down forces. Between the two girders, the magnitudes of the measured principal stresses were similar [-115 MPa (-16.7 ksi) and -68.4 MPa (-9.92 ksi) in the south edge girder, and -94.5 MPa (-13.7 ksi) and -50.4 MPa (-7.31 ksi) in the north edge girder], and directions of the principal stresses were generally symmetrical. The small difference is a result of the asymmetry of the bridge geometry. As the crown is not in the middle, the girders are at different elevations, resulting in the north edge girder having slightly lower stresses than the south edge girder. The measured major principal stresses [-115 MPa (-16.7 ksi) in the south edge girder and -94.5 MPa (-13.7 ksi) in the north edge girder] were much lower than the yield strength of the steel [485 MPa (70 ksi)].

End Floor Beam – Between North Edge Girder and Tie Down

The behavior of the part of the end floor beam between the north edge girder and tie down received particular attention due to the high shear force induced by cable anchoring forces to the north and tie down forces to the south. As shown in Figure 4, the measured direction of the principal stresses in the web of the end floor beam was 60°, compared with 45° for a pure shear stress state. This demonstrates that shear behavior was governing in this region, which was expected. The measured principal stresses [133 MPa (19.3 ksi) and -62.8 MPa (-9.11 ksi)] could help engineers to verify the design stress and have a better understanding of the behavior of locations like this region. Like the edge girders, the measured major principal stress [133 MPa (19.3 ksi)] in this region was much lower than the yield strength of the steel [517 MPa (75 ksi)]. The measurement could also be useful for future inspections. If needed, DIC could be re-deployed at any time.

End Floor Beam – Shop Weld

To the south of the tie down forces, there is a shop weld where the thickness of the web of the end floor beam changes from 0.0381 m (1.5 in.) to 0.0222 m (0.875 in.). This region was monitored to investigate the stresses on the two sides of the shop weld (Figure 5). Figure 5 shows the comparison of the measured principal stresses in the thicker side and the thinner side of the web. The magnitudes of the measured principal stresses increased from the thicker side [104 MPa (15.1 ksi) and 15.0 MPa (2.18 ksi)] to the thinner side [161 MPa (23.3 ksi) and 26.4 MPa (3.83 ksi)], which was expected. The direction of the measured principal stresses decreased from 20° in the thicker side to 5° in the thinner side. As the tie down forces were located closer to the thicker side compared to the thinner side, more shear behavior was expected which resulted in a steeper angle for the principal stresses. Like the other members, the measured major principal stresses [104 MPa (15.1 ksi) in the thicker side and 161 MPa (23.3 ksi) in the thinner side] were much lower than the yield strength of the steel [517 MPa (75 ksi)]. It should be noted that the stress distribution given by DIC, as in Figure 5, could also show the location of the shop weld.

End Floor Beam: Comparison between Measured Data and FE Data

Figure 10 shows the FE predictions for the maximum principal stresses in the end floor beam between the two intermediate stages of construction. These predictions are used to validate DIC measurements and are not reflective of in-situ performance.

As expected, the highest regions of stress are between the north edge girder bearing and the tie down, as well as on the thinner side of the shop weld. Table 1, Table 2, and Table 3 directly compare the measured DIC data with the FE predictions at the location between the north edge girder and the tie down, the shop weld on the thicker side, and the shop weld on the thinner side, respectively. The maximum and minimum principal stresses generally agree, with a peak difference of just 42.7 MPa (6.20 ksi). The angles of these stresses are also close. The differences can be attributed to loads not considered in the local FE model (e.g., temperature), variations between the applied (as-built) loads and the loads used for design, and interactions with members not included in the local FE model (e.g., deck, other floor beams, supplemental longitudinal truss). Overall, this study verifies the DIC findings for this case study.

Supplemental Longitudinal Truss

This research also measured erection-induced stresses in the supplemental longitudinal truss panel between the first and second floor beam next to the end floor beam (Figure 2 and Figure 6). As shown in Figure 6, both sides of the joint were subjected to compression due to the construction procedure. A balanced cantilever construction method was used to build the cable-stayed span (Han et al. 2019). The preassembled modules of the edge girders and the floor system was erected in position, and then the concrete deck was poured (Han et al. 2019). A composite deck system was used to reduce the weight of the deck which reduced the foundation requirement, the section size of the cables, and the capacity of the cranes (Han et al. 2019).

When connected to the end floor beam, the bottom chord of the supplemental longitudinal truss needed to be force fit. This caused compression in the lower chord and the diagonals of the truss, as measured. The stress field in the monitored plate was complicated, as shown in Figure 6. Although stresses were measured in the plate joining the diagonals and lower chord, they can indicate the approximate stresses in the diagonals. The direction of the measured principal stresses [20° on the east side and 55° on the west side] was similar to the direction of the diagonals. The sum of forces in the horizontal direction was only 1.40 MPa (0.203 ksi), which demonstrates the force balance in the horizontal direction. However, the measured principal stresses were -51.4 MPa (-7.45 ksi) and 9.03 MPa (1.31 ksi) on the east side of the plate, and -90.3 MPa (-13.1 ksi) and -33.2 MPa (-4.81 ksi) on the west side of the plate. Besides the construction procedure mentioned above, the existence of tie down forces to the east could also contribute to the lower compressive force on the east side. Although the measured major principal stresses were much less than the yield strength of the steel [485 MPa (70 ksi)], they still demonstrated that the truss carried load from these intermediate construction stages. Therefore, the supplementary longitudinal truss needs to be considered when evaluating the overall behavior of the bridge and when counting on its ability to carry load.

Conclusions

By monitoring the erection-induced strains of the Governor Mario M. Cuomo Bridge, this paper demonstrated the capability and value of implementing DIC to measure the erection-induced strains of long-span bridges. Based on the measured data, the following conclusions are made:

- The measured strains in the two edge girders near the east end floor beam were similar in magnitude and generally symmetrical in direction. The small difference is a result of the asymmetry of the bridge geometry. Higher shear force was measured in the end floor beam between the north edge girder and the tie down, which could help engineers understand the strain field in this member.
- Measured strains on the two sides of the shop weld of the east end floor beam increased from the thicker side to the thinner side. As expected, more shear behavior was measured in the thicker side, as it was closer to the tie down forces.
- Strains were measured in the supplemental longitudinal truss, even though it was not designed to carry load from erection. This indicates that designers should consider erection-induced loads for the design of supplemental longitudinal trusses.
- The measured strains can provide engineers with valuable data on the behavior of built bridges, useful information for inspecting bridges in the long-term, and information that can improve the design of future structures.

The measured data in the three floor beam locations was compared with predictions from a 3D local FE numerical model. The good agreement between the measured and predicted data further verifies 3D DIC as a measurement technique.

As the first implementation of DIC in monitoring the erection-induced strain of a cable-stayed bridge, this research shows the possibility of monitoring full-field strain distributions using DIC, and the unprecedented data DIC can provide on bridge behavior. Recommendations for implementing DIC for monitoring the behavior of bridges during erection include:

- 3D DIC, as opposed to 2D DIC, is recommended as it can capture out-of-plane deformations and it is not necessary to have the camera setup parallel to the measurement area.
- If the DIC setup cannot remain on site during various stages of construction, detailed field notes should be taken such that the DIC setup can be replicated as closely as possible. Using DIC software which can remove rigid body motion is also recommended as it would be nearly impossible to exactly replicate DIC setup locations.
- When monitoring steel components, pressure-activated adhesive tape is recommended as a patterning strategy as it is quick to apply, durable, and is compatible with protective multilayer paint coatings.
- If the measurements need to be taken on different dates and the pattern will be left unattended, communication with the contractor is recommended to make sure that the pattern will not be damaged or removed inadvertently.

This research also highlights the immense potential for DIC to measure dead load and erection-induced strains. While this paper focused on measuring the strains between two intermediate construction stages, it could be used to track behavior from fabrication shops and holding yards to various construction stages to completed bridges with live load. For example, reference frames could be taken at a holding yard as demonstrated for the Governor Mario M. Cuomo Bridge in Figure 11. Additional frames could be taken once these components are erected and then again once the bridge is complete with live load. This would enable a designer, contractor, or owner to understand the as-built behavior of the system. Unfortunately, this could not be demonstrated for this bridge as there was no platform access to the location of the erected member at the time of the research. However, it serves as indicator of future promise of this technology.

Data Availability Statement

All data, models, or code that support the findings of this study are available from the corresponding author upon reasonable request.

Acknowledgements

This work was supported by Dr. Ashley P. Thrall's Myron and Rosemary Noble Associate Professor of Structural Engineering Chair. The authors are grateful to the New York State Thruway Authority for providing the opportunity to perform this research, especially Jamey Barbas and Rajesh Taneja. They appreciate the field support provided by Erik Zuker, Jeremy Velez, Gowen Dishman, Bill VanWart, and Will Torres.

Figure 1. The Governor Mario M. Cuomo Bridge (photo credit: New York State Thruway Authority).

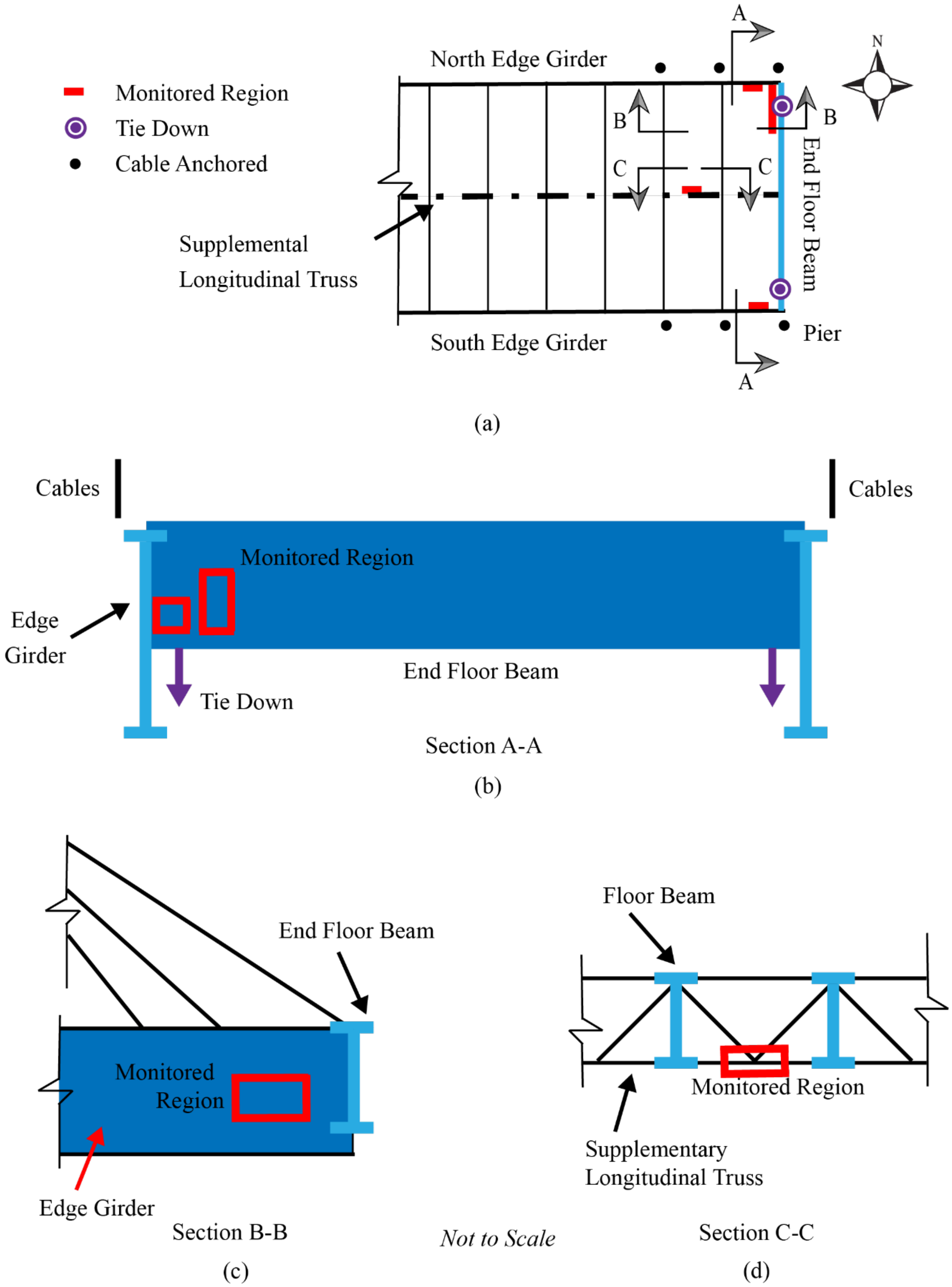

Figure 2. Monitored regions: (a) partial plan view of the bridge; (b) end floor beam; (c) edge girder; (d) supplemental longitudinal truss.

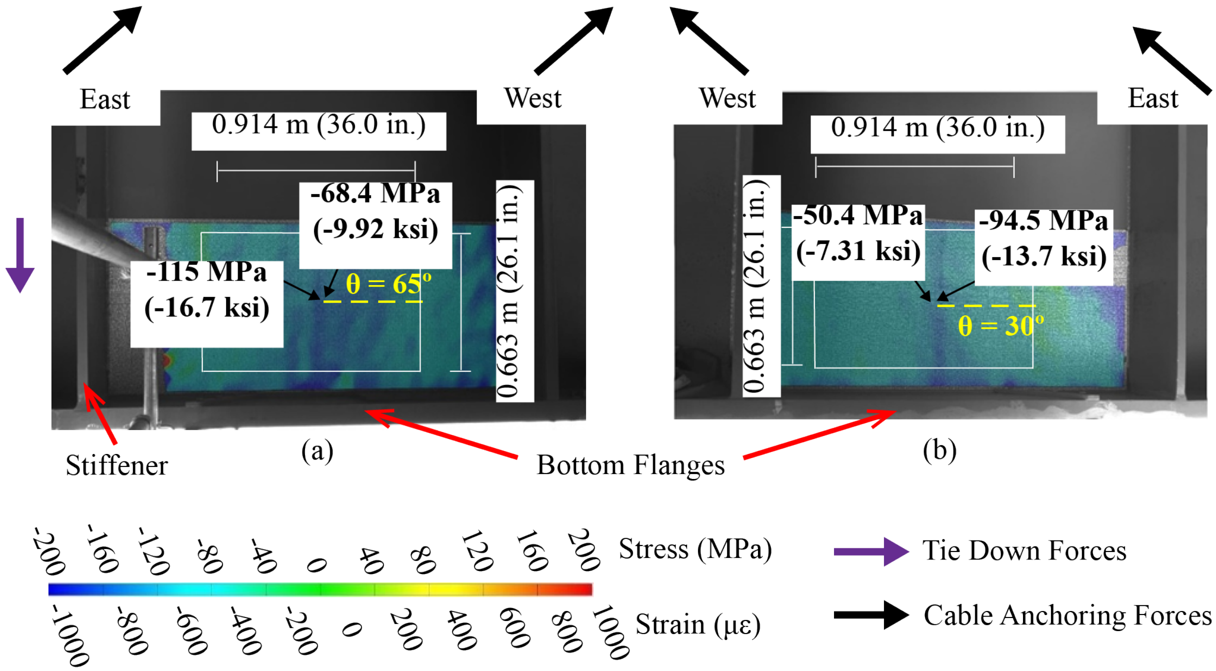

Figure 3. Measured full-field stress distribution in the principal stress direction of edge girders: (a) south edge girder; (b) north edge girder.

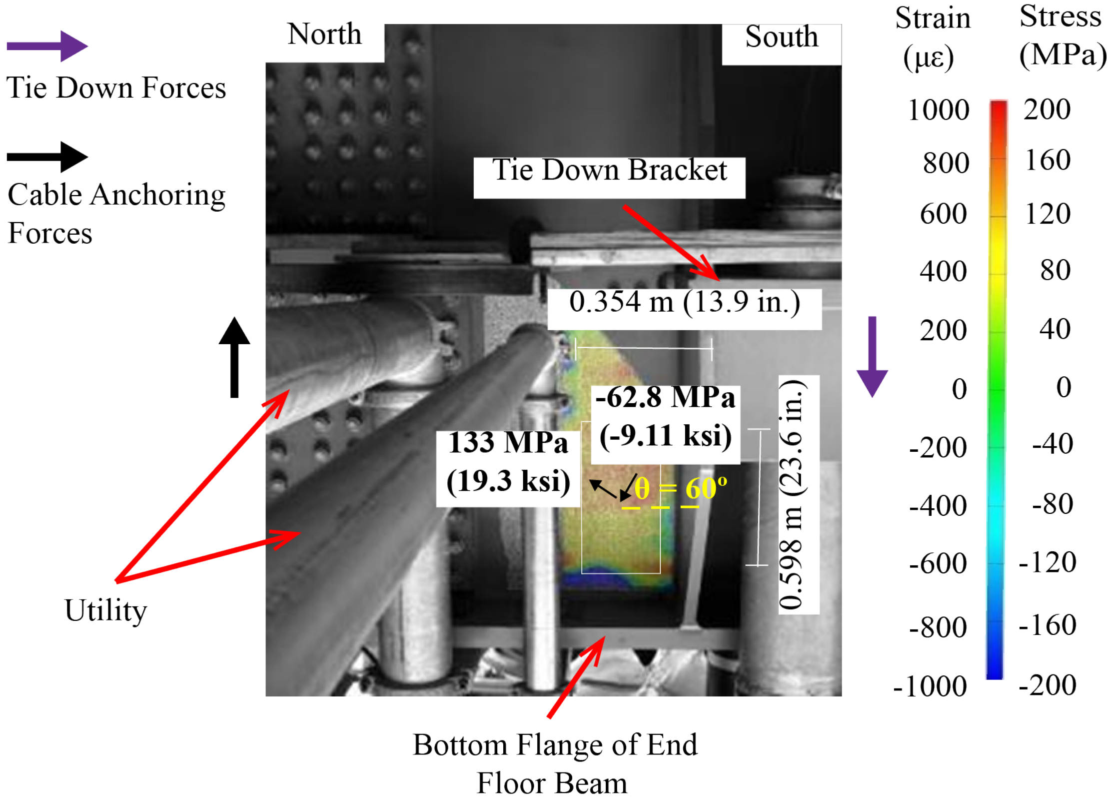

Figure 4. Measured full-field stress distribution in the principal stress direction of the location between the north edge girder and the tie down.

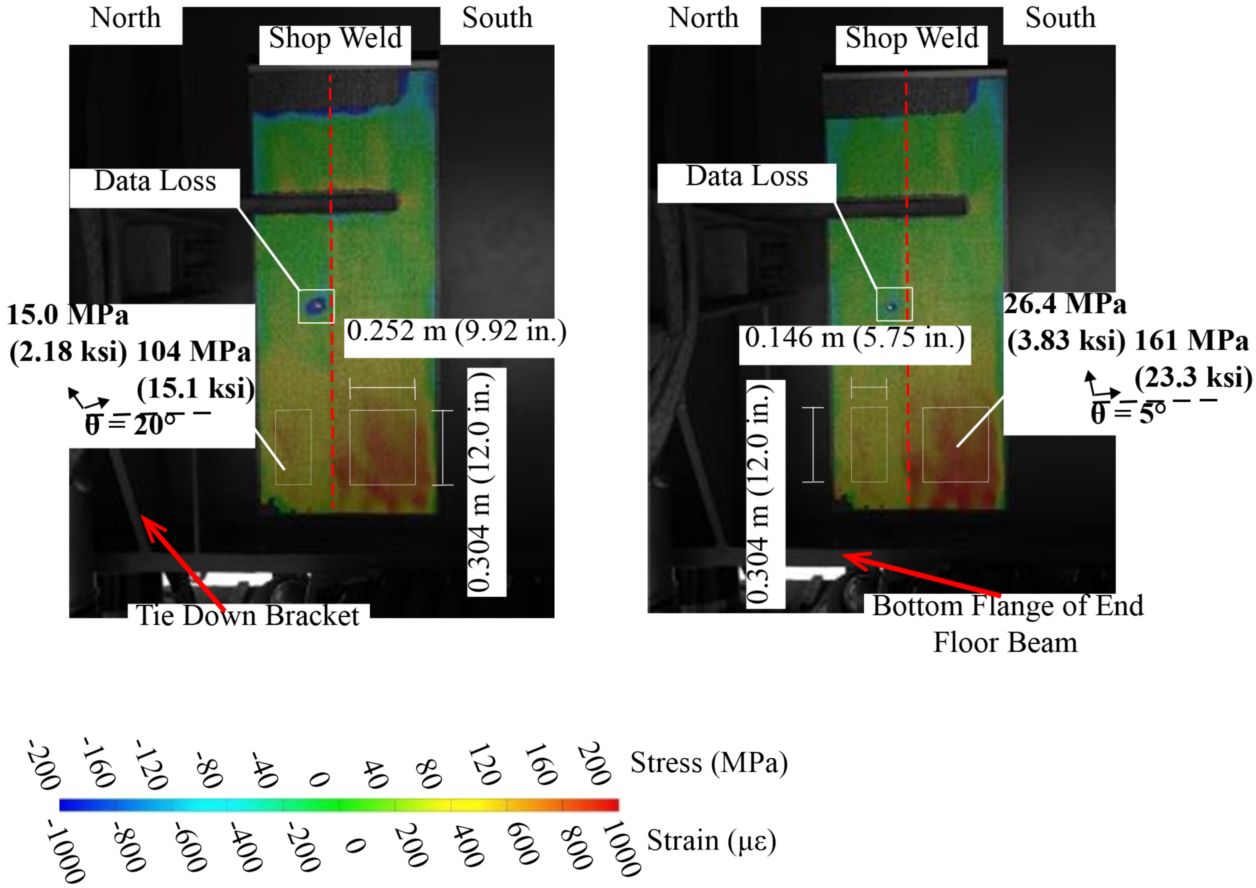

Figure 5. Measured full-field stress distribution in the principal stress direction at the location of the shop weld.

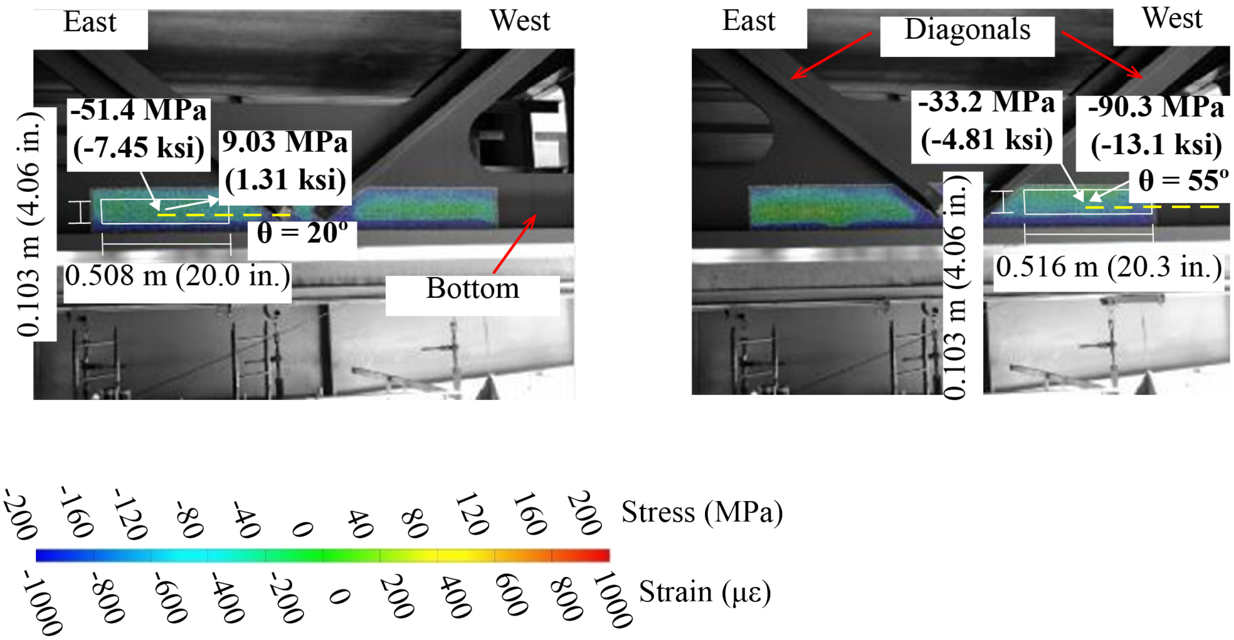

Figure 6. Measured full-field stress distribution in the principal stress direction in the supplemental longitudinal truss.

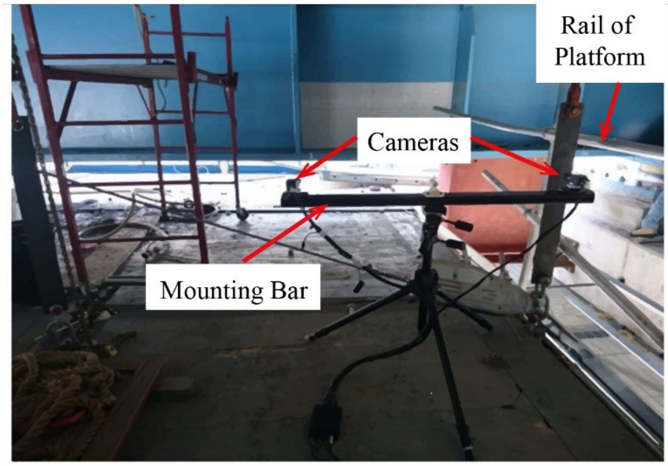

Figure 7. 3D DIC system.

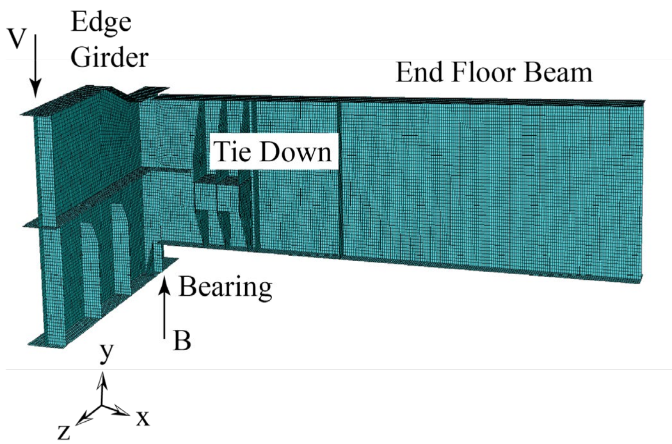

Figure 8. FE model of end floor beam.

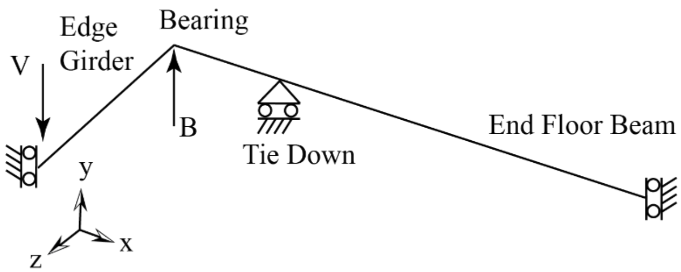

Figure 9. Free body diagram.

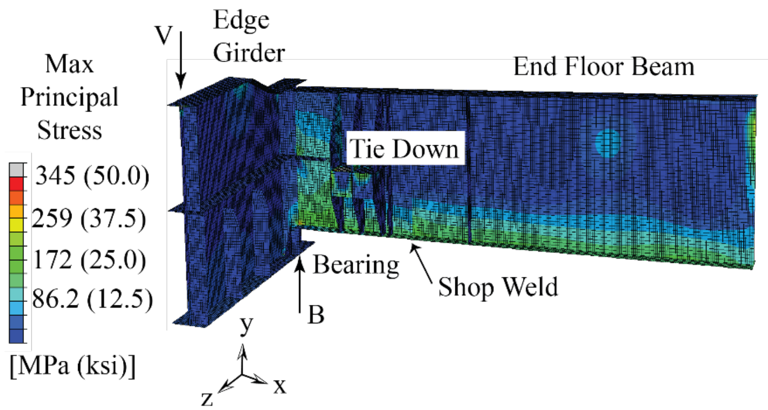

Figure 10. FE predictions of maximum principal stresses in the end floor beam.

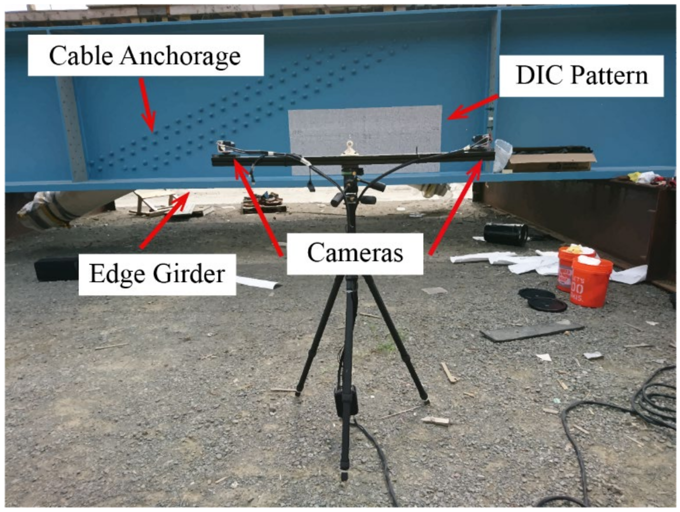

Figure 11. Taking DIC photographs before erection.

Table 1. End Floor Beam – Between North Edge Girder and Tie Down: Measured and FE predictions of principal stresses and angle.a

	Measured	FE	Difference (absolute value)
Maximum Principal Stress [MPa (ksi)]	133 (19.3)	148 (21.4)	14.5 (2.10)
Minimum Principal Stress [MPa (ksi)]	-62.8 (-9.11)	-66.1 (-9.58)	3.24 (0.470)
Angle, Θ (degrees; defined in Figure 4)	60	54.5	5.50

Table 2. End Floor Beam – Shop Weld (Thicker Side): Measured and FE predictions of principal stresses and angle.

	Measured	FE	Difference (absolute value)
Maximum Principal Stress [MPa (ksi)]	104 (15.1)	80.0 (11.6)	24.1 (3.50)
Minimum Principal Stress [MPa (ksi)]	15.0 (2.18)	0.0848 (-0.0123)	15.1 (2.19)
Angle, Θ (degrees; defined in Figure 5)	20	-1.78	21.8

Table 3. End Floor Beam – Shop Weld (Thinner Side): Measured and FE predictions of principal stresses and angle.

	Measured	FE	Difference (absolute value)
Maximum Principal Stress [MPa (ksi)]	161 (23.3)	122 (17.7)	42.7 (6.20)
Minimum Principal Stress [MPa (ksi)]	26.4 (3.83)	-2.87 (-0.416)	29.3 (4.25)
Angle, Θ (degrees; defined in Figure 5)	5	-1.02	6.02

References

ABAQUS. 2022. *ABAQUS/Standard.* Waltham, MA: Dassault Systemes.

ARAMIS User Manual. 2017. GOM, Braunschweig, Germany.

Baldoni, J., Lionello, G., Zama, F., and Cristofolini, L. 2016. "Comparison of different filtering strategies to reduce noise in strain measurements with digital image correlation." *Journal of Strain Analysis for Engineering Design*. 51(6):416-430.

Barbas, J., and Paradis, M. 2019. "Scalable, modularized solutions in the design and construction of the Governor Mario M. Cuomo Bridge." *Structural Engineering International*, 29(1):123-127.

Barton, F.W., Baber, T.T., Ramsey, R.D., and McKeel, Jr., W.T. 1990. "Measured stresses in the deck segments of a cable-stayed bridge, Bridge Evaluation, Repair and Rehabilitation" In *Proceedings of the NATO Advanced Research Workshop on Bridge Evaluation, Repair and Rehabilitation*, 187 NATO ASI Series:421-433.

Casas, J.R., and Aparicio, A.C., 1998. "Monitoring of the Alamillo Cable-stayed Bridge during construction." *Experimental Mechanics*, 38(1):24-28.

Gikas., V., Karydakis, P., Piniotis, G., Mpimis, T., Papadimitriou, F., and Panagakis, A. 2014. "Design and implementation of a multi-sensor monitoring system for structural integrity assessment: the case of Attiki Odos, Pallini cable-stayed bridge." In *Proc. of IBSBI 2014*.

Gonzalez, R.C., and Woods, R.E. (2008). *Digital Image Processing* (third ed.), Pearson, New York.

Han, D., and Sun, C. 2003. "Construction control of the Yamen Cable-stayed Bridge." In *Proc. of 3rd International Conference on Current and Future Trends in Bridge Design*, Construction and Maintenance, 268–274.

Han, J., Martello, M., and Wright, K. 2019. “Bridging the Hudson.” *Civil Engineering*, 89(9):54-61.

Hu, J., Sun, X., and Jiao, S. 2012. “Monitoring of long-span self-anchored arch bridge constructed with rotation method.” *Applied Mechanics and Materials*, 178-181.

Kim, S.W., Cheung, J.H., Park, J.B., and Na, S.O. 2020. “Image-based back analysis for tension estimation of suspension bridge hanger cables.” *Structural Control and Health Monitoring*. 27, e2508.

Kim, S.W., Jeon, B.G., Cheung, J.H., Kim, S.D., and Park, J.B. 2017. “Stay cable tension estimation using a vision-based monitoring system under various weather conditions.” *Journal of Civil Structural Health Monitoring*. 7:343-357.

Kim, S.W., Jeon, B.G., Kim, N.S., and Park, J.C. 2013. “Vision-based monitoring system for evaluating cable tensile forces on a cable-stayed bridge.” *Structural Health Monitoring.* 12(5-6):440-456.

Kleinhans, D. 2010. “Monitoring during bridge widening.” *Railway Track & Structures*, 106(3):33-38.

Koller, I. 1997. “Non-destructive testing of Hungarian steel bridges during their erection” in: Structural assessment: the role of large and full-scale testing. CRC Press, Florida, pp. 124-131.

Koo, K.Y., Brownjohn, J.M.W., List, D.I., and Cole, R. 2013. “Structural health monitoring of the Tamar suspension bridge.” *Structural Control and Health Monitoring*, 20:609-625.

Malite, M., Takeya, T., Gonçalves, R.M., and de Sáles, J.J. 2018. “Monitoring of the Paraná River Bridge during launching.” *Structural Engineering International*, 3:193-196.

Mathew, M.D., Ellenberg, A., Esola, S., McCarthy, M., Bartoli, I., and Kontsos, A. 2018. "Multiscale deformation measurements using multispectral optical metrology." *Structural Control and Health Monitoring*. 25, e2166.

McCormick, N., and Lord, J. 2012. "Digital image correlation for structural measurements." In *Proc. of ICE - Civil Eng*. 165(4):185-190.

McGinnis, M.J., Smith, B.J., Holloman, M., Lisk, M., O'Donnell, A., and Kurama, Y.C. 2012. "3-D digital image correlation—an underused asset for structural testing." In *Proc. of 2012 Struct. Congr.*, 1958-1969.

Molina-Viedma, A.J., Pieczonka, L., Mendrok, K., López-Alba, E., and Díaz, F.A. 2020. "Damage identification in frame structures using high-speed digital image correlation and local modal filtration." *Structural Control and Health Monitoring*. 27, e2586.

Oliveira Pedro, J.J., and Reis, A.J. 2010. "Nonlinear analysis of composite steel-concrete cable-stayed bridges." *Engineering Structures*, 32:2702-2716.

Pan, B., Qian, K., Xie, H., and Asundi, A. 2009. "Two-dimensional digital image correlation for in-plane displacement and strain measurement: a review." *Measurement Science and Technology*, 20(6): 062001.

Palanca, M., Tozzi, G., and Critofolini, L. 2016. "The use of digital image correlation in the biomechanical area: a review." *International Biomechanics*. 3(1):1-21.

Piniotis, G., Gikas, V., Mpimis, T., and Perakis, H. 2016. "Deck and cable dynamic testing of a single-span bridge using radar interferometry and videometry measurements." *Journal of Applied Geodesy*. 10(1):87–94.

Schlaich, M. 2001. “Erection of cable-stayed bridges having composite decks with precast concrete slabs.” *Journal of Bridge Engineering*, 10.1061/(ASCE)1084-0702(2001)6:5(333), 333-339.

Schmidt, T., Tyson, J., and Galanulis, K. 2003a. “Full-field dynamic displacement and strain measurement using advanced 3D image correlation photogrammetry: Part I.” *Exp Tech*. 27(3): 47-50.

Schmidt, T., Tyson, J., and Galanulis, K. 2003b. “Full-field dynamic displacement and strain measurement using advanced 3D image correlation photogrammetry: Part II.” *Exp Tech*. 27(4): 22-26.

Schmidt, T., and Tyson, J. 2004. “Full-field dynamic displacement and strain measurement using pulsed and high-speed 3D image correlation photogrammetry.” *SEM 2005 Conference Proceedings,* Portland OR.

Shahawy, M.A., and Arockiasamy, M. 1996a. “Analytical and measured strains in Sunshine Skyway Bridge II.” *Journal of Bridge Engineering*. 10.1061/(ASCE)1084-0702(1996)1:2(87).

Shahawy, M.A., and Arockiasamy, M. 1996b. “Field instrumentation to study the time-dependent behavior in Sunshine Skyway Bridge I.” *Journal of Bridge Engineering*, 10.1061/(ASCE)1084-0702(1996)1:2(76).

Somja, H., and de Ville de Goyet, V. 2008. “A new strategy for analysis of erection stages including an efficient method for creep analysis.” *Engineering Structure*, 30:2871-2883.

Sony, S., Laventure, S., and Sadhu, A. 2019. “A literature review of next-generation smart sensing technology in structural health monitoring.” *Structural Control and Health Monitoring*. 26, e2321.

Sutton, M. A., Orteu, J. J., and Schreier, H. 2009. *Image Correlation for Shape, Motion and Deformation Measurements; Basic Concepts, Theory and Applications*, Springer, New York, NY.

The New NY Bridge, About the project. 2020. Accessed April 26, 2020. https://www.newnybridge.com/about/.

The New NY Bridge, Iconic opening. 2018. Accessed April 28, 2020. https://www.newnybridge.com/iconic-opening-governor-cuomo-announces-eastbound-span-opening/.

Trilion. 2020. "2D vs 3D Digital Image Correlation." Accessed April 25, 2022. http://faq.trilion.com/docs/2d-vs-3d-digital-image-correlation/

Wang, Y., Thrall, A.P., Baah, P., and Strain, R. 2022. "Behavior of steel girder bridges subjected to vehicular collision." *Engineering Structures*, 255: 113929.

Wang, Y., Thrall, A.P., and Zoli, T.P. 2021. "Behavior of the Delaware River Bridge during repair." *Journal of Constructional Steel Research*. 177:106448.

Wang, Y., Tumbeva, M.D., Thrall, A.P., and Zoli, T.P. 2019. "Pressure-activated adhesive tape pattern for monitoring the structural condition of steel bridges via digital image correlation." *Structural Control and Health Monitoring*. e2382.

Weinmann, T.L., and Huey, P. 2015. "Long bridge widening and truss lift monitoring." In *Proc. of Structures Congress 2015*, 10.1061/9780784479117.028.

Wu, Q-X, and Chen, B.C. 2008. "Construction monitoring of Xiyangping Bridge in Zhangzhou, China." In *Proc. of Chinese Croatian Joint Colloquium Long Arch Bridges*, 383-392.

Yamamoto, T., and Kitahara, T. 1986. Quality control in the erection of cable-stayed bridge, IABSE reports, 51:259-266.

Ye, X.W., Ni, Y.Q., Wai, T.T., Wang, K.Y., Zhang, X.M., and Xu, F. 2013. “A vision-based system for dynamic displacement measurement of long-span bridges: algorithm and verification.” *Smart Structures and Systems*. 12(3-4):363-379.

Zhou, G.D., Yi, T.H., and Chen, B. 2017. “Innovative design of a health monitoring system and its implementation in a complicated long-span arch bridge. *Journal of Aerospace Engineering*, 10.1061/(ASCE)AS.1943-5525.0000603.